J Mater Sci: Mater Electron (2026) 37:872

Exploring lithium ion transport efficiency in modified MgO-supplementary PVdF-HFP nanocomposite polymer electrolytes: Intuitions from Electrochemical study

G. Vijayakumar[1,*], B. Rajani[2], N. Sukumar[3], N. Rajiv Chandar[4], V. Sapna[1], P. Selvakumar[5], Vellaiappillai Tamilavan[6], and M. Ponnusamy[7]

[1] *Department of Chemistry, Vivekanandha College of Engineering for Women(Autonomous), Tiruchengode, Namakkal, Tamil Nadu 637205, India*
[2] *Department of Electrical and Electronics Engineering, Aditya College of Engineering and Technology, Aditya University, Surampalem, Andhra Pradesh 533437, India*
[3] *Department of Chemistry, Shree Venkateshwara Hi-Tech Engineering College, Gobichettipalayam, Tamil Nadu, India*
[4] *Department of Physics, Coimbatore Institute of Technology, Affiliated to Anna University, Coimbatore 641013, India*
[5] *Department of Chemistry, Nehru Institute of Technology, Coimbatore, Tamil Nadu 641 105, India*
[6] *Department of Physics, Pukyong National University, Busan 608737, Republic of Korea*
[7] *Department of Chemistry, J K K Munirajah College of Technology, T.N Palayam, Tamil Nadu, India*

Received: 25 January 2026
Accepted: 7 April 2026

© The Author(s), under exclusive licence to Springer Science+Business Media, LLC, part of Springer Nature, 2026

ABSTRACT

Modified MgO (*m*MgO) incorporated thin film poly (vinylidenefluoride-co-hexafluoropropylene) (PVdF-HFP) nanocomposite polymer membrane (TFPM) have been fabricated by simple phase inversion technique. *m*MgO nanofiller (8*wt. %* loading) treated PVdF-HFP polymer matrix improved in porosity (ϱ) up to 81%. The TFPM have better mechanical strength (2380 kPa) than untreated polymer membrane (1310 kPa). Thermal properties of 8*wt.%* *m*MgO loaded TFPM achieved better results in T_m, T_g, ΔH_m and X_c values such as 141.7 °C, − 43.3 °C, 23.84 $J.g^{-1}$ and 22.76% than other (≤ 6*wt. %* loading) TFPMs. TFPMs were immersed in *y*$LiClO_4$ + EC/DMC (1:1 by volume) separately to form a thin film nanocomposite polymer membrane electrolyte (TFPE). Lithium ion conductivity of TFPE was obtained 3.1×10^{-3} S cm^{-1} and the Li^+ transference number was found to be a maximum of ca. 0.79. The finding TFPE [MCMB||TFPE|| $LiCoO_2$] provided an avenue for LIBs, which can be a potential candidates for energy storage devices technology.

Address correspondence to E-mail: ngvijayakumar@gmail.com

https://doi.org/10.1007/s10854-026-17228-6
Published online: 21 April 2026

1 Introduction

In the present century, composite polymer membrane electrolytes have gained significant research interest for their application in storage devices, notably lithium-ion batteries and fuel cells. The performance of high-rate LIBs is strongly dependent on the enhancement of Li^+ conductivity in the electrolyte and charge transfer kinetics at the electrodes [1]. The rechargeable LIBs are found to have a common role not only in power backup but also in hybrid electric vehicle (HEV) uses. The global LIB market, valued at USD 4.76 billion in 2016, is projected to expand to USD 25.47 billion by 2025, largely driven by hybrid electric vehicles (57.6%) and consumer electronics (21.5%). LIBs are widely recognized for their high energy density, long cycle life, light weight design, high single-cell voltage, and absence of memory effect, with each property strongly influenced by the choice of electrode–electrolyte materials. LIBs have been universally utilized which includes digital cameras, tablets, computers and laptops, smart mobile phones etc., [2–5]. Electrochemical behaviors of such batteries will be accomplished as anticipated not only by preferable electrodes but also by suitable membrane electrolytes. The electrolyte preparation is still one of the most challenging and most important for battery researchers in terms of physical and electrochemical characteristics. Typically, polymer membrane electrolytes are significant and dependent upon Li^+ ion movement between electrodes during the charging and discharging process. Researchers have generally chose various polymer matrixes to prepare porous polymer membrane electrolytes, reasonably interesting in ion conducting, compatibility of polymers such as polyethylene oxide (LiTFSI–PI-PEO) [6], Polyvinyl chloride (PVC-NH_4SCN-glycerol) [7], poly(acrylonitrile-methyl-methacrylate) (PAN-MMA-$LiBF_4$-EC + GBL) [8], Poly (vinyl alcohol) (PVA-PMMA- $LiBF_4$) [9], poly (methyl methacrylate) (PMMA-MgO-$LiClO_4$) [10], poly(methyl methacrylate-co-acrylonitrile) P(MMA-AN-SnO_2) [11], poly(vinylidene fluoride (PVdF) [12], poly(vinylidene fluoride—hexa fluoro propylene) / poly(ethylene terephthalate) (PVdF-HFP/ PET) [13], and poly(vinylidene fluoride – co -hexa fluoropropylene / polyacrylonitrile) PVdF-HFP / PAN) [14] and poly (vinylidene fluoride – co- hexa fluoro propylene) (P(VdF – co – HFP)) [15–17], etc. are considered a healthier matrix. In composite membranes, co-polymer segments positioned along pore walls help form continuous VdF-rich channels within the porous structure, facilitating Li^+ conduction. Furthermore to the interfacial stability, nanofillers too show great salvation competence with gel-type polymer electrolyte and high affinity in addition to transporting the capacity of Li^+ ion. Recently, Nanofiller added composite polymer electrolytes have been established which is due to various enhancements in electrochemical characteristics due to present energy demands. One-dimensional Al_2O_3 nanofillers optimized composite electrolyte based on a poly(vinylidene fluoride-co-hexafluoropropylene) (PVDF-HFP), and plastic crystal plasticizer succinonitrile exhibits an impressive ionic conductivity of 6.46×10^{-4} S cm^{-1} and the cells delivered a high discharge capacity of 158.2 mAh g^{-1} at 0.1 C [18]. Sulfonated PVDF-HFP and SiO_2 based quasi-solid-state composite electrolyte (QSE) showed a lithium transference number of 0.66 at 30 °C. [19]. ZrO_2-incorporated PVDF-HFP/LiTFSI matrix achieved that reduces in crytallinity which boost Li^+ conductivity of 9.26×10^{-5} S.cm^{-1} at 30 °C which offered better mechanical strength (3.23 MPa) and very good flame safety among all of them [20]. Electrochemical impedance spectroscopy revealed that the impact of 2% blend hausmannite nanofiller on PVDF–HFP/PEG blend nanocomposite polymer electrolytes (NCPE) exhibited the highest ion conductivity of 3.1×10^{-4} S cm^{-1} at 80 °C, an order of magnitude higher than the pristine NCPE (5.1×10^{-5} S cm^{-1}) [21]. The use of a nanocomposite microporous PE, especially PVdF-HFP based TiO_2 [22, 23], Al_2O_3 [24], nm SiO_2, fumed SiO_2 [25, 26], MgO [27], and CeO_2 [28] on the polymer matrix better performance, in its place of conventional liquid electrolyte and may considerably enhance the protection purpose of lithium batteries. Various lithium salts such as $LiBF_4$, $LiCF_3SO_3$, $LiClO_4$, LiTFSI, and $LiFePO_4$ have been explored, among which $LiClO_4$ is considered highly promising due to its superior electrochemical stability and ability to deliver high energy density [29–31]. Polymer plasticization is another established strategy to enhance ionic conductivity by increasing segmental chain mobility and amorphous content [32]. Incorporation of plasticizers such as EC, DMC, PC, or PEG has been shown to improve dielectric properties, generate more free charge carriers, and boost ionic mobility within the polymer matrix [33–36]. Moreover, Polymer electrolytes are not limited to lithium salts; there is growing interest in Na^+, Mg^{2+}, Al^{3+}, Ca^{2+}, and K^+etc., and other multivalent cations expected for next-generation energy storage due to abundance, low cost,

and safety advantages. Beyond polymer electrolytes based on Li^+ ion batteries, other metals salts like Na^+, Mg^{2+}, Al^{3+}, Ca^{2+}, K^+, etc. reported by battery researcher. For instance, Sodium-based polymer electrolytes, such as $NaPF_6$ incorporated in PEO, exhibit promising ionic conductivity on the order of ~ 10^{-4} S cm^{-1}. [37]. Mg^{2+} based gel polymer electrolytes, particularly those employing PVdF-HFP/PMMA blends, demonstrate high electrochemical stability and dendrite-free Mg^{2+} deposition, enabling safer multivalent battery systems, with an initial discharge capacity of 100.6 mAh g^{-1} that gradually decreases over 10 cycles [38]. Ca and Al -based electrolytes have attracted attention for high-capacity multivalent energy storage systems; however, attaining sufficiently high ionic conductivity remains a significant challenge. In this context, the calcium analogue $Ca[Al(HFIP)_4]_2$ dissolved in dimethoxyethane (DME) has emerged as a promising electrolyte candidate for calcium-ion battery applications [39, 40]. Experimental verification of the computationally designed Na and K based polymer electrolytes reveals ionic conductivities reaching ~ 1.0×10^{-3} S cm^{-1} at 80 °C and Na^+ transference number of approximately 0.57. Furthermore, electrochemical cycling of a Na|2:1 NaFSI/PolyIL|Na symmetric cell exhibited a low overpotential of ~ 100 mV at 0.5 mA cm^{-2}, along with stable sodium plating/stripping behavior for over 100 h.[41]. But, lithium based batteries have only reached high energy density and long durability than other above said Na^+, Mg^{2+}, Al^{3+}, Ca^{2+}, and K^+ batteries.

Many research works were undertaken to enhance the LIBs without liquid electrolytes. Given serious thrust, several investigations have explored preparing solid, composite and gel-based polymer electrolytes with lithium salts, plasticizers, polymer materials, and all including polymer electrolytes. Among these approaches, first time synthesis of modified MgO incorporated in PVdF-HFP polymer matrix successfully by phase inversion technique. The prepared thin film composite polymer membrane as well as thin film composite polymer electrolyte showed better result in mechanical stability, physical as well as electrochemical performance. The performances of the composite polymer electrolyte have been achieved by the combination of composite polymer membrane, lithium perchloride ($LiClO_4$) and addition of mixture of plasticizers (EC and DMC). TFPEs have been used in combination with MCMB anode and $LiCoO_2$ cathode to fabricate MCMB||TFPE|| $LiCoO_2$ which have been applied and enhanced the electrochemical behavior such as Li^+ transference, interfacial stability and charge–discharge characteristics too. Considerable research efforts are thus being directed toward the development of all-solid or gel-based polymer electrolytes as safer and more efficient alternatives to liquid systems for next-generation LIBs.

2 Experimental details

2.1 Materials

Poly(vinylidene fluoride-co-hexafluoropropylene) (PVdF-HFP, Mw ≈ 40,000), 3-(2,3-epoxypropoxy) propyltrimethoxysilane, and lithium perchlorate ($LiClO_4$) were procured from Sigma Aldrich (USA) and used as received. The MgO nanoparticles employed in this study were synthesized following the procedure reported elsewhere [42]. Prior to use, $LiClO_4$, MgO, and the copolymer matrix were thoroughly dried under vacuum (10^{-1} Torr) at 100 °C maximum 12 h to eliminate residual moisture. N-methyl-2-pyrrolidone (NMP) was supplied by E-Merck (Germany), while ethylene carbonate (EC) and dimethyl carbonate (DMC), obtained from Sigma Aldrich, served as plasticizers and were used without further purification.

2.2 *Modified* MgO *and mMgO -PVdF-HFP thin film membrane preparation:*

The synthetic routes for modified magnesium oxide (*m*MgO) nanoparticles have obtained by simple soft chemical method. First, 3-(2,3-Epoxypropoxy)-propyl]-trimethoxysilane was dissolved in a 95% C_2H_5OH solution, with a 1:4 v/v ratio of the silane agent to the ethanol–water mixture, and magnetically stirred ambient temperature for 10 – 15 min to form Solution I. In parallel, nano magnesium oxide particles were scattered in double distilled water, thoroughly mixed, and stirred to ensure uniform wetting resulting in Solution II. Solution I was added drop wise way to solution II under constant stirring for 12 h. After the stirring process was complete, the mixture was filtered and the product was dried at 100 °C before being ground into a fine powder to yield the *m*MgO NPs [42, 43]. Further, it was fully characterized by XRD, TEM and FTIR.

The host polymer PVdF-HFP was dissolved in NMP at 45 °C under continuous stirred for 24 h to form a homogenous mixture solution. *m*MgO NPs (*wt%* = 0,

2, 4, 6, 8 and 10) were added to the polymer matrix in appropriate weight percentages to create a homogenous slurry. Following duration of 12 to 18 h, the polymer nanocomposite solution evolved into viscous slurry. A range of thin film nanocomposite PVdF-HFP polymer membranes was produced using the phase inversion technique, as detailed in prior studies [44]. By drying each membrane, a solvent-free thin film polymer composite membrane termed "thin film nanocomposite *m*MgO- based PVdF-HFP polymer membrane (TFPM)" was obtained. The thicknesses of the TFPM were obtained in the range of 30–60 µm measure by micrometer. The thin film nanocomposite *m*MgO-based PVdF-HFP polymer electrolytes, referred to as TFPE, were produced by soaking the TFPM in 1 M $LiClO_4$ in EC/DMC (1:1 by volume) for around 6 to 8 h in an inert atmosphere. Figure 1 shows the schematic representation of TFPE preparation to LiBs. The thicknesses of the TFPE were obtained in the range of 40–70 µm. Moreover, impact of varying lithium salt concentrations ($y$$LiClO_4$, where, y corresponds to 0.25, 0.5, 0.75, and 1.0 M concentration) with EC/DMC (1:1 by volume) was explored to optimize the *m*MgO NPs in TFPM system [8*wt*% *m*MgO + 92*wt*% PVdF-HFP]. After optimization of TFPM, both the physical as well as mechanical characteristics of the TFPM and the electrochemical characteristics of the TFPE were assessed.

2.3 Physical Characterization

The thermal behavior of TFPMs were investigated through differential scanning calorimetry (DSC) employing a Perkin Elmer Pyris DSC-6 system. The samples were examined under a nitrogen environment with a programmed heating rate of 10 °C min^{-1}. The porosity and electrolyte uptake of the polymer electrolytes were characterized and the procedure where described elsewhere [28]. The electrolyte solution uptake (ESL) of the TFPEs was evaluated by sandwiching the membrane between two filter papers and applying pressure using a 100 g PTFE sheet. The samples were subjected to an applied pressure of ~ 133.322 × 10^{-2} Pa, and their weight was recorded at intervals of 10 min [43]. XRD patterns of the mMgO and TFPE were investigated by X-ray diffractometer (JEOL, Model: JDX) using nickel filtered Cu-K radiation between 10° to 80° at 2° min^{-1}. *m*MgO NPs was characterized by Fourier-transform infrared spectroscopy (FTIR) and were recorded with a Nicolet 380 spectrophotometer in the wavelength range 4000–400 cm^{-1}. The morphology of the optimized TFPE images (representative sample) was investigated using a field emission scanning electron microscopy (FE-SEM, JSM-6340F, JEOL) operated at an accelerating voltage of 20 kV.

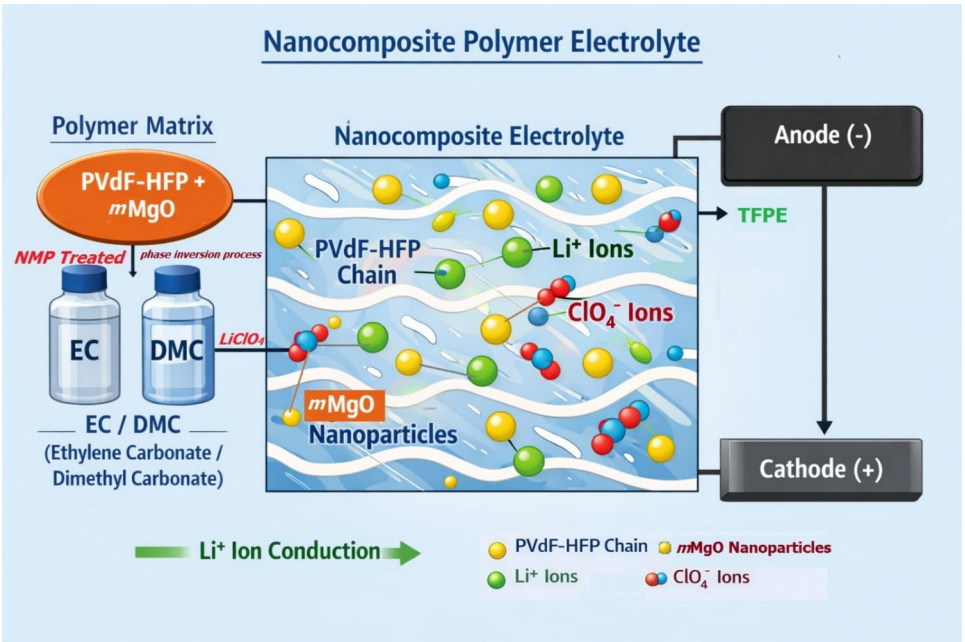


Fig.1 Schematic diagram of preparation of TFPE

2.4 Electrochemical characterization

The electrochemical behavior of the dried TFPM was assessed by soaking it in a non-aqueous electrolyte consisting of 1 M $LiClO_4$ in EC/DMC (1:1 by volume) for 6–12 h, resulting in the formation of TFPE. Following activation, the membrane was carefully removed, and any residual electrolyte on its surface was gently blotted with filter paper. To study the ionic conductivity, TFPE samples were prepared with varying $LiClO_4$ concentrations (y = 0.25, 0.5, 0.75, and 1.0 M) in the optimized polymer electrolyte containing 8 *wt*% *m*MgO nanofiller. The bulk resistance (Rb) was determined by sandwiching the membrane between two stainless steel (SS) non-blocking electrodes and recording the response using a computer-controlled LCR HiTESTER (HIOKI 3522–50). Impedance spectra were obtained with a 10 mV AC perturbation over the frequency range of 0.1 Hz to 100 kHz, and the ionic conductivity (σ) was calculated using Eq. (1).

$$\sigma = l/R_b \times A \tag{1}$$

Here, l and A denote the thickness of the polymer electrolyte membrane and the electrode area, respectively [29]. The transference number was determined following a previously reported method [28]. To minimize moisture interference, all electrochemical tests were performed inside an argon-filled glove box.

The interfacial stability of TFPE was further examined using a symmetric Li/TFPE/Li cell configuration on an EG&G electrochemical analyzer. Impedance measurements were carried out within the frequency range of 10 Hz to 100 kHz using a 10 mV perturbation, and the stability was monitored over different storage intervals under an inert argon atmosphere.

A 2032 coin-type lithium-ion polymer cell (MCMB||TFPE|| $LiCoO_2$) was fabricated by placing the TFPE electrolyte layer between a mesocarbon microbead (MCMB) anode and a $LiCoO_2$ cathode. All experiments were carried out in an argon-filled inert atmosphere. The electrochemical performance of the cell was examined galvanostatically using a WonATech battery cycle life tester. Cycling tests were conducted at a C/2 rate with a constant current density of 0.25 mA cm^{-2}, within the potential window of 3.0–4.2 V.

3 Results and discussion

3.1 Modified MgO confirmation studies

Figure 2 presents the XRD patterns of both pristine MgO and *m*MgO NPs synthesized at 100 °C for 1 h. The observed diffraction peaks at (111), (200), (220), and (222) confirm the crystalline nature of the samples and are characteristic of the cubic phase of MgO, matching the standard JCPDS card no. 04–0829. The lattice constant was calculated to be approximately 0.421 nm, and the average crystallite size was estimated to be around 20 nm using the Scherrer equation [42, 43].

Figure 3 illustrates the transmission electron microscopy (TEM) image of the MgO and surface- *m*MgO NPs. TEM analysis revealed that *m*MgO NPs exposed hazy appearances owing to the surface modification, though modification process have been done on MgO, the NPs remained independent and have seen few agglomerations. The crystalline natures retained after surface modification has done on the MgO NPs at 100 °C. Spherical shape and size less than 50 nm with stony like outside attributed that few aggregations of *m*MgO NPs were the ranges between 34.2 nm and 62.7 nm in size than unmodified MgO (Fig. 3a).

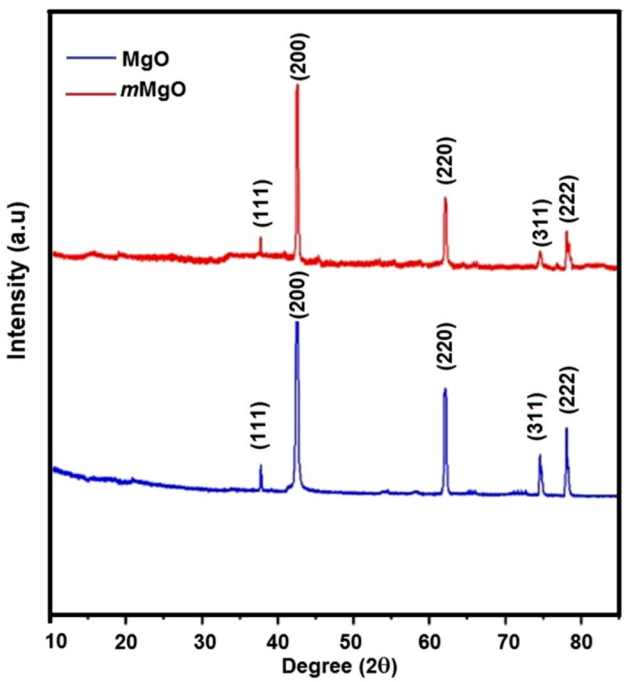


Fig. 2 XRD pattern of MgO and mMgO NPs

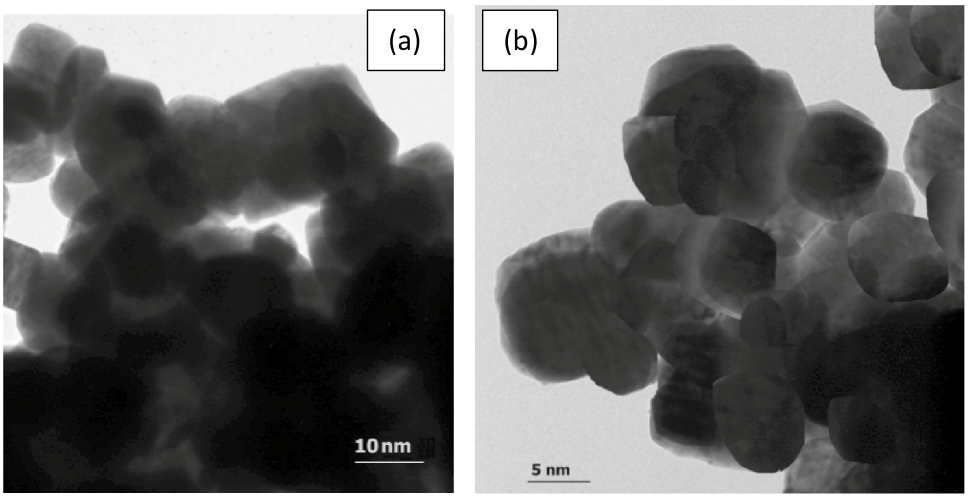


Fig. 3 TEM image **a** MgO and **b** mMgO NPs

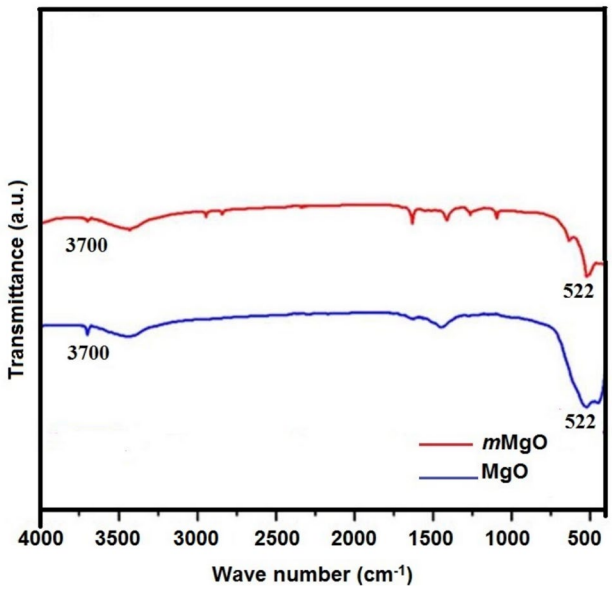


Fig.4 FTIR analysis of MgO and mMgO NPs

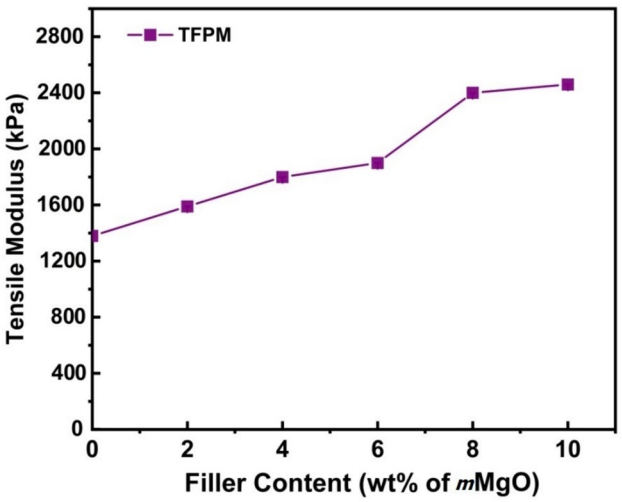


Fig. 5 Mechanical strength of the TFPM (*wt*% of *m*MgO = 0, 2, 4, 6, 8,&10)

The FTIR spectrum of *m*MgO NPs, demonstrates a weaker band at 3700 cm^{-1} compared to the spectrum of MgO showed in Fig. 4. This observation suggested that a reduction in hydroxyl groups density on the surface of *m*MgO NPs, indicating that modification process utilizing hydroxyl groups was successfully carried out [42]. The broad peak observed around 3500 cm^{-1} in both MgO and mMgO FTIR spectra corresponds to the stretching vibration of surface –OH groups. This is typical for metal oxides and indicates the presence of surface hydroxyls, which can influence filler–polymer interactions. The sharp peaks in the 2000–1000 cm^{-1} range correspond to Mg–O lattice vibrations, while the broad –OH peak is distinct and informative for surface chemistry." Therefore, Lewis acid sites (O-vacancies) are bound to ClO_4^- anions through coordination and separate the Li^+ ClO_4^- pairs to thus produce dissociated Li^+ ions which serve as charge carriers.

3.2 Mechanical integrity

Mechanical performance of the TFPMs as a function of *m*MgO nanofiller concentration is illustrated in Fig. 5. A progressive enhancement in tensile strength was observed with increasing nanofiller content, which is primarily attributed to the strong interfacial interaction between the inorganic *m*MgO NPs

and the PVdF-HFP polymer chains. The pristine PVdF-HFP membrane exhibited a tensile strength of 1310 kPa following phase inversion. With the incorporation of *m*MgO NPs, the tensile modulus showed a steady rise, reaching a maximum of 2380 kPa at 8*wt*% loading. Beyond this concentration, a slight improvement to 2460 kPa was recorded, likely due to the onset of nanoparticle agglomeration, which may hinder uniform stress distribution. These findings emphasize the significance of optimized nanofiller dispersion in enhancing the mechanical robustness of TFPMs, which is vital for maintaining structural integrity and reliability during electrochemical cycling.

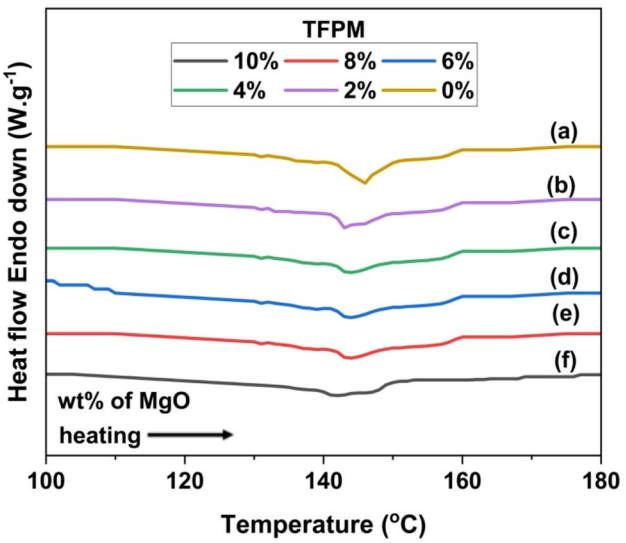


Fig. 6 DSC analysis of TFPM **a** 0 *wt*% **b** 2 *wt*% **c** 4 *wt*% **d** 6 *wt*% **e** 8 *wt*% **f** 10 *wt*% *m*MgO incorporated PVdF-HFP based composite membrane (TFPMs)

3.3 Thermal DSC analysis

Differential Scanning Calorimetry (DSC) analysis was performed to investigate the crystallinity and thermal behavior of the pristine PVdF-HFP membrane as well as TFPMs with varying *m*MgO NPs (0, 2, 4, 6, 8 and 10 *wt* %) content. The crystallinity (*Xc*) value obtained 45.51% for the pristine TFPE (0wt% *m*MgO loaded). As shown in Fig. 6 and summarized in Table 1, the degree of crystallinity (*Xc*) decreased notably from 33.2% for the (2 *wt* %) minimum *m*MgO loaded membrane to 22.3% for the 10 *wt*% *m*MgO loaded TFPM. Correspondingly, the enthalpy of fusion (ΔH_m) was reduced from 34.77 J g^{-1} for the (2*wt* %) minimum *m*MgO loaded membrane to 23.84 J g^{-1} maximum 10 *wt*% *m*MgO NPs loaded membrane, indicating the disruption of crystalline domains due to *m*MgO nanofiller incorporation.

Additionally, the glass transition temperature (T_g) of the optimized system shifted to –43.3 °C, compared to –39.4 °C in the unfilled membrane. This reduction suggests enhanced polymer chain flexibility, primarily due to favorable interactions between the *m*MgO nanofillers and the PVdF-HFP chains, as well as improved compatibility within the polymer matrix [36].

3.4 Porosity, electrolyte solution uptake and solution leakage studies

The correlation between the percentage of porosity and the *m*MgO nanofiller content present in TFPMs is depicted in Fig. 7. Table 1 shows the measured porosity values of the samples. *m*MgO NPs concentration upto 8*wt*% was increased the porosity by

Table 1 Physical and thermal studies on TFPM to optimize *m*MgO nanofiller on the polymer matrix

TFPM	T_m (°C)	ΔH_m ($J.g^{-1}$)	X_c (%)	T_g (°C)	SL *wt* (%)	ρ (%)	ESU *wt* (%)	Film Strength
TFPM1	143.6	47.63	45.51	−39.4	33	52	77	Good
TFPM2	143.2	34.77	33.20	−41.1	30	64	184	Good
TFPM3	142.9	28.53	27.24	−41.6	28	66	190	Excellent
TFPM4	142.1	26.63	25.43	−42.4	25	75	203	Excellent
TFPM5	141.7	23.84	22.76	−43.3	20	81	215	Excellent
TFPM6	142.5	23.35	22.30	−42.7	22	79	188	Good

Phase inversed thin film polymer membranes are denoted as TFPM1 = 0*wt*% *m*MgO + 100*wt*% PVdF-HFP; TFPM 2 = 2*wt*% *m*MgO + 98*wt*% PVdF-HFP; TFPM 3 = 4*wt*% *m*MgO + 96*wt*% PVdF-HFP; TFPM4 = 6*wt*% *m*MgO + 94*wt*% PVdF-HFP; TFPM 5 = 8*wt*% *m*MgO + 92*wt*% PVdF-HFP; TFPM 6 = 10*wt*% *m*MgO + 90*wt*% PVdF-HFP, ρ = % ± 0.5%

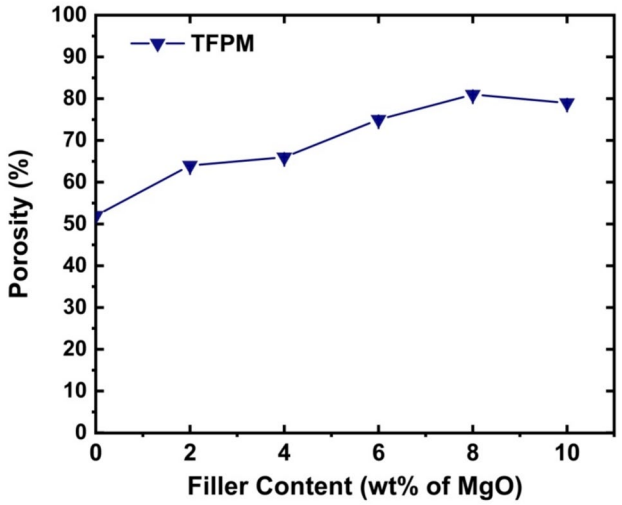


Fig. 7 Porosity of TFPM with various loading *wt%* mMgO nanofiller

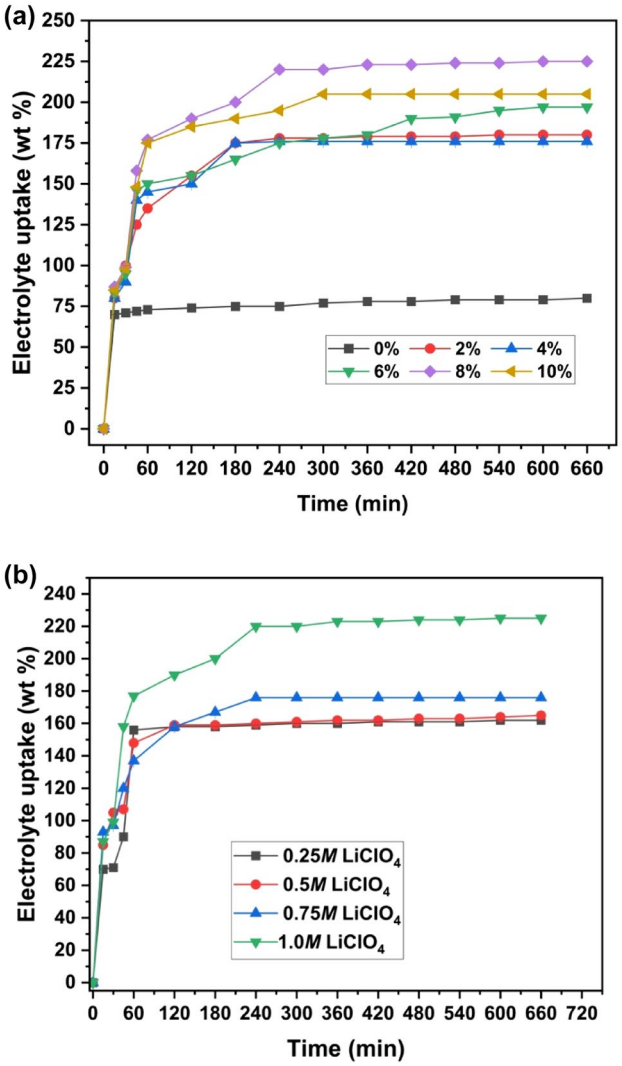


Fig. 8 **a** Electrolyte uptake of TFPM with various loading *wt%* mMgO (*wt%* = 0, 2, 4, 6, 8 & 10). **b** Electrolyte uptake of the optimized (8*wt%* *m*MgO) nanofiller loaded TFPM with various lithium salt *y*$LiClO_4$(*y* = 0.25 M, 0.5 M, 0.75 M and 1.0 M) concentration

nearly 81% ± 0.5%, but further increases in nano filler content led to a 79% ± 0.5%, slight reduction due to aggregation of *m*MgO and steric hindrance. Moreover, surface to volume ratio of the *m*MgO nanofiller caused a sharp rise in membrane porosity, as seen in the polymer matrix from 2 *wt* % to 8 *wt%* *m*MgO than pristine TFPM, concentration with some continued expansion.

Figure 8a highlights the electrolyte solution uptake (ESU) of the TFPMs, showing the nanofiller which tend to elevate electrolyte uptake (225 *wt%* ± 1%, around < 240 min). It reaches the optimized level beyond that values showed 188% ± 1%, a decline in uptake after around 300 min which may be due to reaching the saturation level *m*MgO concentration on the polymer membrane. It is also attributed that 8*wt%* *m*MgO loaded on the electrolyte which has attained surface-to-volume ratio of TFPM. As clearly shown in Fig. 8b, the optimized TFPM with various electrolyte concentration studies observed that 1 M LiClO4 electrolyte uptake reached 215 *wt%* ± 1%, better than all other lithium salt (0.25, 0.5 and 0.75 M LiClO4) concentration systems (from 156 ± 1%, to 166 *wt%* ± 1%).

The electrolyte solution leakage (SL) behavior of TFPEs is presented in Fig. 9a. For the 8 *wt%* *m*MgO-loaded sample, leakage stabilized at ~ 20% ± 0.5%, after 40 min, indicating strong interactions between the nanofiller, polymer framework, and lithium salt electrolyte. In contrast, the 10 *wt%* *m*MgO system exhibited a marginally higher leakage (~ 22% ± 0.5%), which can be ascribed to nanofiller agglomeration and reduction in porosity of the membrane. Figure 9b illustrated the solution leakage with various lithium salt electrolyte concentrations which showed leakage has reduced 20 *wt%* ± 0.5%, at 1 M LiClO4 than other TFPEs (24 *wt%* ± 0.5%, 26 *wt%* *wt%* ± 0.5%, and 23 *wt%* ± 0.5%, from 0.25 M, 0.5 M and 0.75 M LiClO4) showed in Table 2. Hence, the solution leakage is restricted by not only influenced by the membrane's porous nature but also the interaction of the optimum concentration of the electrolyte on membrane surface.

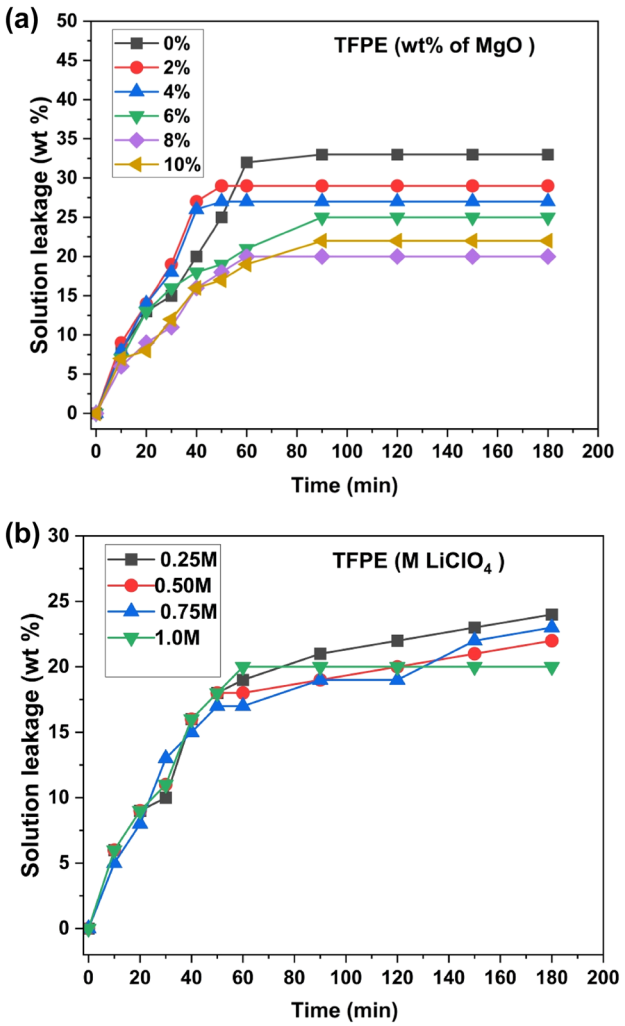


Fig. 9 a Solution leakage of TFPM with various loading *wt%* *m*MgO NPs (*wt%* = 0, 2, 4, 6, 8, &10). **b** Solution leakage of the optimized (8*wt%* *m*MgO NPs) nanofiller loaded TFPM with various lithium salt *y*$LiClO_4$ concentration (*y* = 0.25 M, 0.5 M, 0.75 M and 1.0 M)

3.5 Morphological description

The surface morphologies of the selected TFPEs, captured by FE-SEM, are illustrated in Fig. 10 (a–d). When comparing the TFPM soaked in different electrolyte concentration, it was originated that the TFPE texture had to have an asymmetric structure, very tiny pores ~ 2 µm, maximum TFPE showing sub micrometer pores < 1 µm and some areas of places were seen to be non-porous on the membrane (Fig. 10a–d). TFPE texture shows a compact structure and electrolytes are disbursed in the composite polymer matrix, few rough surfaces were observed may be evidence that enhancing the strength of the film and tiny pores are distributed among the surface which may be due to homogenously distributed magnesia with no aggregates seen on the polymer matrix (Fig. 10a–d). TFPM exhibits sub-microporous as well as microporous structure rather than a solid structure [43].

3.6 Ionic conductivity studies

The ionic conductivity of TFPEs was investigated at 25 °C as a function of nanofiller concentration. As illustrated in Fig. 11, the addition of *m*MgO up to 8 *wt%* led to a progressive enhancement in conductivity, attaining a maximum of 3.1 mS cm^{-1}. Beyond this loading, a minor decline was observed (down to 2.8 mS cm^{-1}), which can be attributed to the dominant influence of dilution at higher filler levels [43]. Beyond that this behavior is consistent with the porosity, solvent uptake, and leakage results (Figs. 7, 8, 9), where the optimized TFPE exhibited superior characteristics compared to other compositions reported [45]. A summary of the room-temperature conductivities of phase-inverted TFPEs is provided in Table 3, highlighting their favorable performance. Furthermore, DSC analysis confirmed that phase inversion in TFPM lowered the degree of crystallinity, increasing

Table 2 Thermal studies on TFPE with optimized *m*MgO content

TFPE	T_m (°C)	ΔH_m ($J.g^{-1}$)	X_c (%)	T_g (°C)	SL *wt (%)*	ESU *wt (%)*
TFPE1	133.5	22.62	21.12	− 34.43	24	156
TFPE2	133.8	21.54	20.34	− 35.17	26	158
TFPE3	133.4	19.71	19.47	− 36.21	23	166
TFPE4	131.7	17.84	16.76	− 37.39	20	215

TFPE [92*wt%*(PVdF-HFP + 8*wt%* *m*MgO + *y*$LiClO_4$ + EC /DMC ((*v/v*) 1:1)]; $LiClO_4$ concentration various such as TFPE1, *y* = 0.25 M; TFPE 2, *y* = 0.5 M; TFPE 3, *y* = 0.75 M; TFPE4, *y* = 1 M, respectively. SL in *wt%* ± 0.5%; ESU in *wt%* ± 0.5%

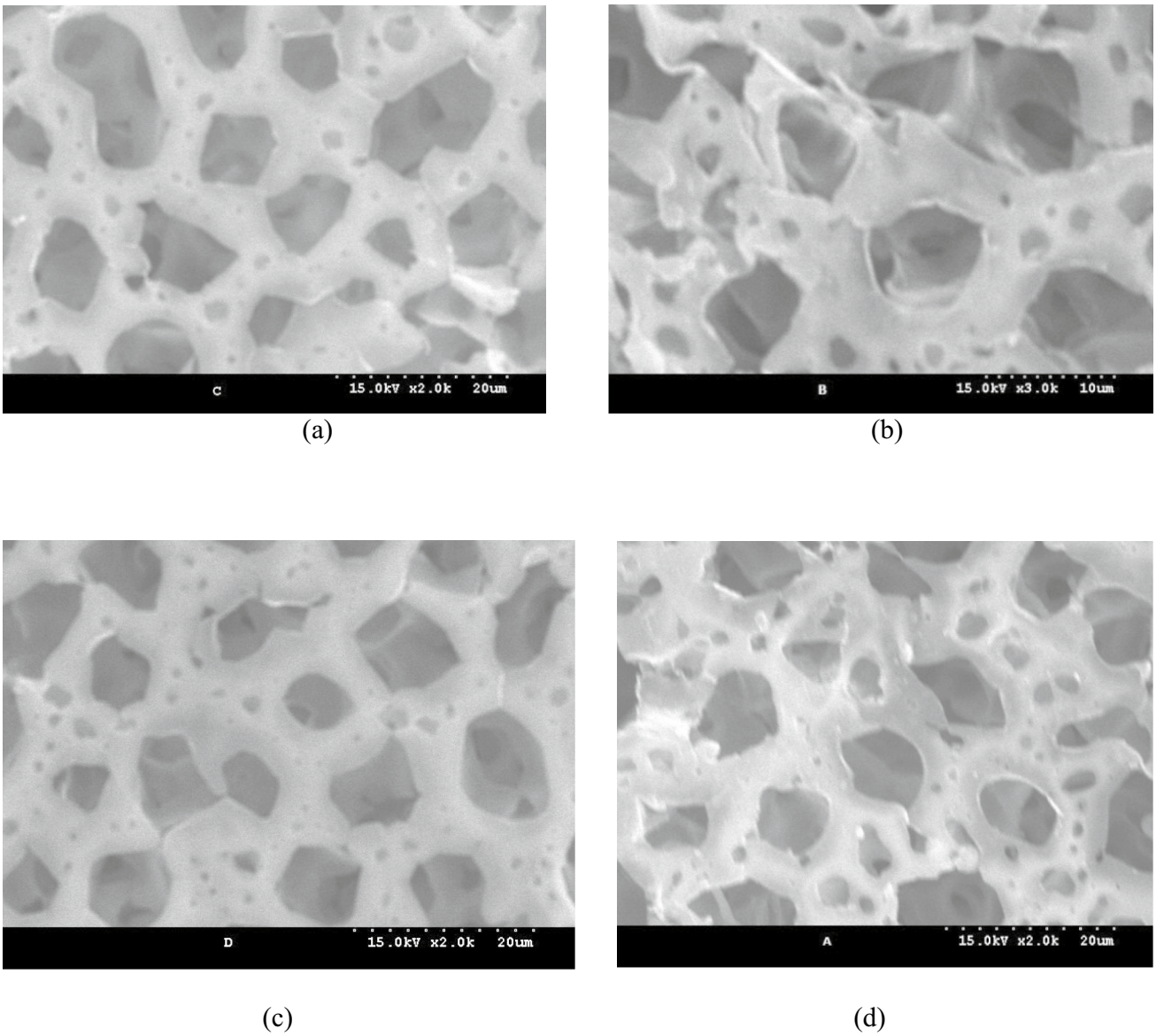


Fig. 10 FE-SEM images of optimized TFPE with varying *y*$LiClO_4$ Concentration **a** 0.25 M **b** 0.5 M **c** 0.75 M and **d** 1.0 M $LiClO_4$

amorphous regions and thereby facilitating more efficient ion transport through the polymer matrix during electrochemical operation, which substantiates the observed improvement in conductivity.

3.7 Effect of thermal variation on ionic conductivity

The temperature-dependent ionic conductivity of TFPEs is presented in Fig. 12a, b showing a notable rise in log (conductivity), with the highest performance observed for the TFPE4 sample. This system demonstrated improved liquid electrolyte absorption, reaching up to 215% with the addition of 8 *wt*% *m*MgO. However, beyond this concentration, further addition of *m*MgO nanofiller resulted in a sharp decrease in electrolyte uptake—by nearly 27%—likely due to filler aggregation hindering membrane porosity. At higher filler contents, a dilution effect dominated, causing a reduction in overall ionic conductivity [13]. The initial conductivity enhancement can be attributed to efficient charge carrier mobility, polymer swelling interactions [31, 32], and partial crystallization within the composite structure. As illustrated in Fig. 13, the improved

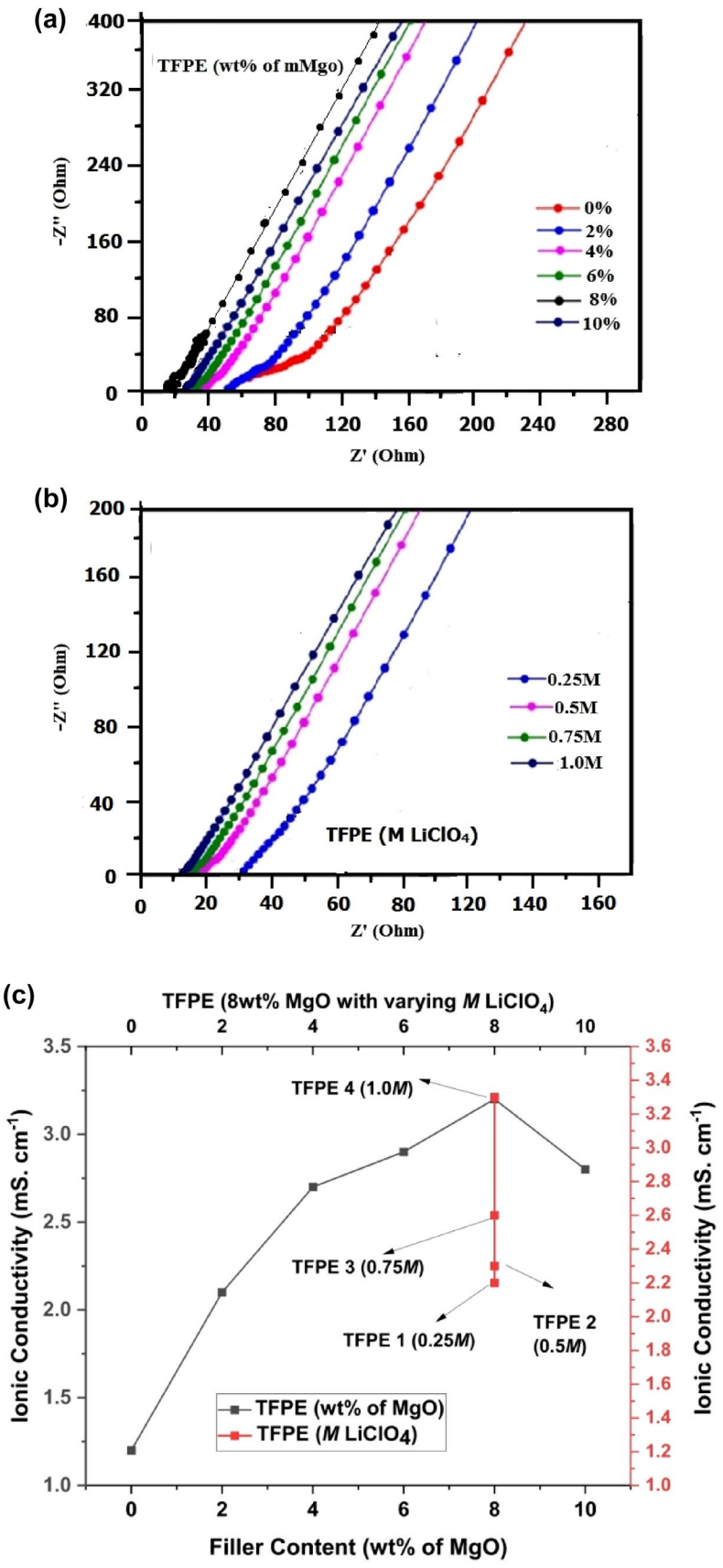


Fig. 11 **a** Nyquist plot of TFPE with various *wt%* *m*MgO NPs. **b** Nyquist plot of TFPE with *y*$LiClO_4$ Concentration i)TFPE1 ($y = 0.25$ M) ii) TFPE2 ($y = 0.5$ M) iii) TFPE3 ($y = 0.75$ M) and iv) TFPE4 ($y = 1.0$ M). **c** Room temperature ionic conductivity of the TFPE *vs* various *wt%* of *m*MgO NPs (dark black line) and optimized *m*MgO NPs nanofiller *vs* varying in $LiClO_4$ concentration (red line)

Table 3 Electrochemical properties of TFPE to optimize the nanofiller content

*m*MgO *(wt%) in TFPE*	σ (mS.cm^{-1})	I_o (μA)	I_s (μA)	R_o (Ω)	R_S (Ω)	Time (sec)	T_+	Film Strength
0	1.2	42.3	26.7	258.93	497.86	5100	0.52	Good
2	2.1	28.4	21.2	159.7	53.4	3600	0.63	Excellent
4	2.7	33.6	20.1	153.7	240.3	3600	0.64	Excellent
6	2.9	34.7	19.3	168.5	259.4	3300	0.65	Excellent
8	3.1	23.1	16.5	159.9	226.1	3200	0.79	Excellent
10	2.8	29.7	19.4	176.8	281.0	3800	0.64	Good

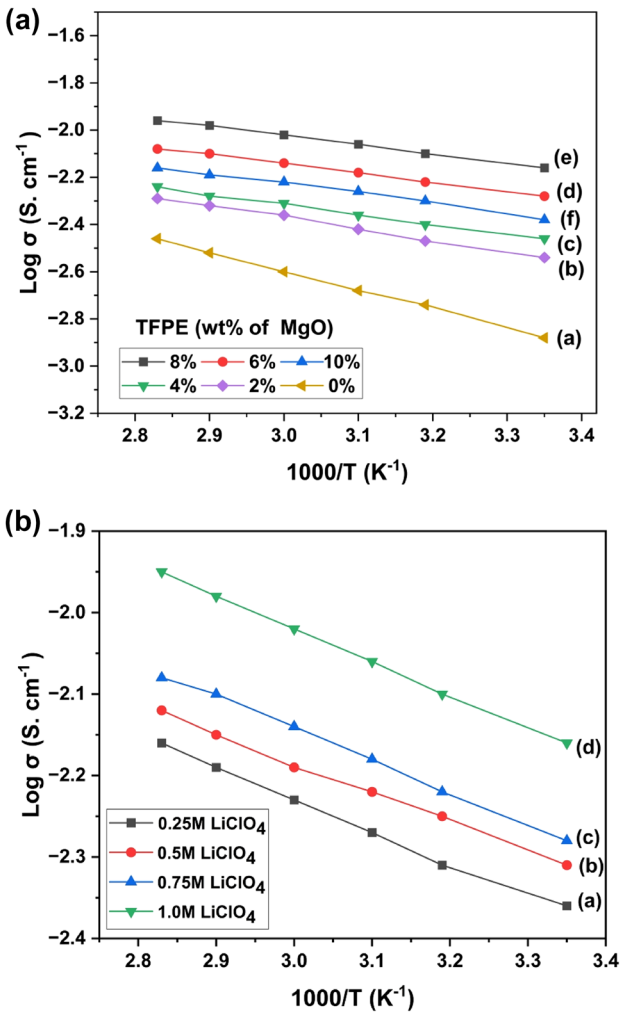


Fig. 12 **a** Temperature dependence on ionic conductivity of TFPE with various *wt%* (**a**) 0% (**b**) 2% (**c**) 4% (**d**) 6% (**e**) 8% and (**f**) 10% of *m*MgO NPs. **b** Temperature dependence ionic conductivity of the TFPE with *y*$LiClO_4$ **a** TFPE1 ($y=0.25$ M) **b** TFPE2 ($y=0.5$ M) **c** TFPE3 ($y=0.75$ M) and **d** TFPE4 ($y=1.0$ M)

conductivity is further supported by the synergistic interaction among *m*MgO NPs, the polymer matrix, and the lithium salt, facilitating ion transport.

3.8 XRD studies of TFPE

XRD Pattern TFPE with various *wt* % of *m*MgO is shown in the Fig. 14. Pristine TFPE (0wt% *m*MgO NPs) showed semi crystalline nature. *m*MgO NPs on PVdF-HFP matrix revealed that TFPE were moved a transition from a semi-crystalline to more amorphous phase. Inclusion of the *m*MgO NPs were from 2 to 10*wt*% significantly suppresses the crystallinity of the PVdF-HFP membrane (Fig. 14), as evidenced by the reduced diffraction peak intensities, indicating an expansion of the amorphous phase [44]. However, at higher filler loadings (> 8 *wt*%), ion-pair dissociation decreases due to increased *m*MgO NPs aggregation and stronger coordination between the PVdF-HFP chains and attributed to induce Li^+ ions, which restricts ionic mobility. The reduction in crystallinity is primarily governed by interfacial interactions within the PVdF-HFP/ *m*MgO NPs – $LiClO_4$ system. Modified MgO boost the Lewis acid base interaction between them. Since lithium-ion transport predominantly occurs through the amorphous regions, which provide greater free volume, enhanced amorphization facilitates ion migration [43]. Consequently, the increased amorphous content contributes to improved ionic conductivity, promotes porous structure formation, and enhances the overall electrochemical performance.

3.9 Interfacial stability studies

Evaluating the interfacial stability between TFPE and lithium metal electrodes is crucial for ensuring reliable performance in electrochemical systems. Electrochemical impedance spectroscopy (EIS) was conducted on seven symmetric Li/TFPE/Li non-blocking cells over varying storage durations. The interfacial resistance values were derived from the diameter of the semicircles in the impedance spectra,

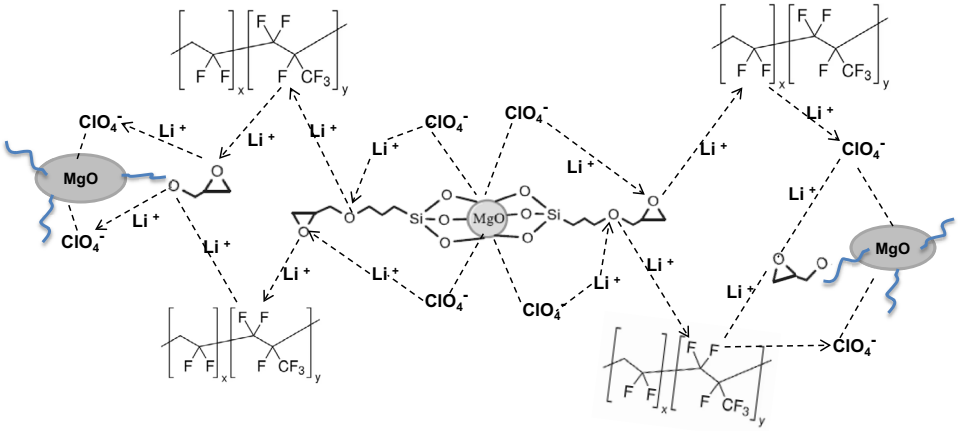


Fig. 13 Lithium-ion interaction mechanism between PVdF-HFP, $LiClO_4$ and Lewis acid base interaction of *m*-MgO NPs

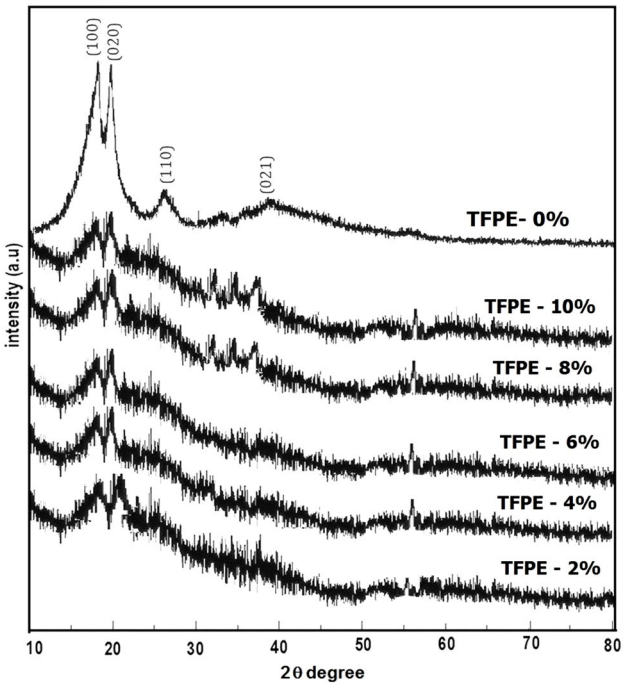


Fig. 14 XRD pattern of TFPE with various wt% of *m*MgO

and the variation of resistance with storage time is illustrated in Fig. 15a, b. As shown, the interfacial resistance for the optimized TFPE containing 8 *wt*% *m*MgO increased from 84 Ω·cm^2 to 252 Ω·cm^2 over a 720 h (30 day) period, suggesting strong interfacial adhesion between the polymer membrane and lithium metal. The gradual increase in resistance over time may result from the formation of a passivation layer on the lithium surface and the progressive degradation of physical contact at the polymer–lithium interface [16, 28]. Among the tested compositions,

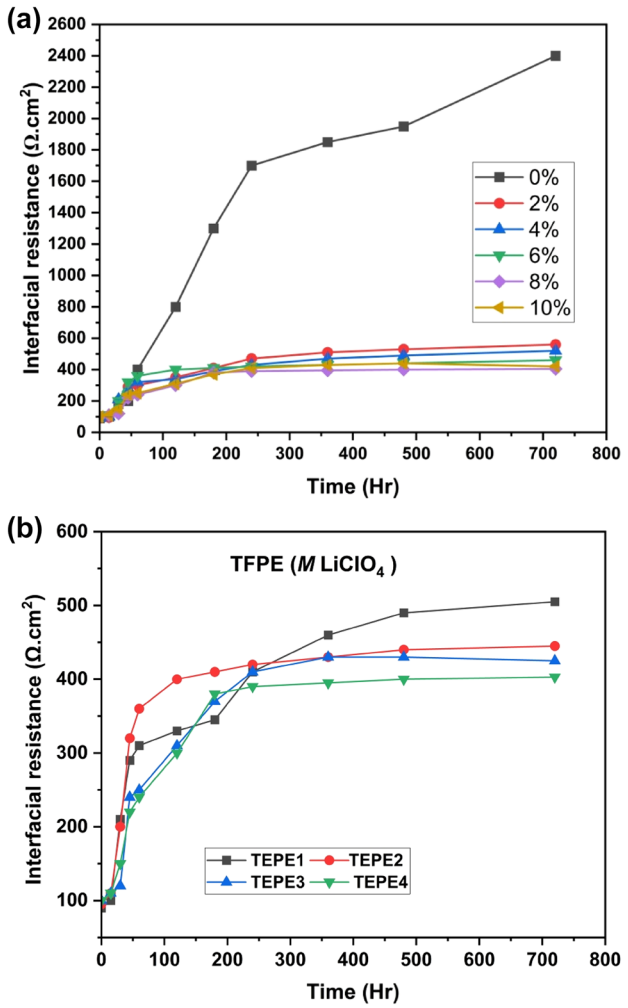


Fig. 15 a Interfacial resistance of the TFPE with various *wt*% of *m*MgO NPs (*wt* %=0%, 2%, 4%, 6%, 8% and 10% **b** Interfacial resistance of the optimized *m*MgO NPs in TFPE at different concentrations of *y*$LiClO_4$ (y=0.25 M, 0.5 M, 0.75 M and 1 M)

the TFPE with optimized filler loading exhibited the most stable interfacial behavior.

3.10 Transference number studies

It is further essential to determine the transference number of Li^+ ion for TFPEs and their data given in Table 3. The chronoamperometry analysis of the TFPE containing the optimized filler concentration revealed an initial current (I_0) of 23.1 μA, as shown in Fig. 16a–d. The current was tracked over time under a small DC polarization of 10 mV, reaching a steady-state value (Is) of 16.5 μA at approximately 3200 s. Corresponding AC-impedance measurements yielded values of R_0 = 159.9 Ω and Rs = 226.1 Ω. A voltage (ΔV) was applied across the TFPE layer positioned between two lithium non-blocking electrodes, a method suitable for correcting the effects of surface passivation [29]. Table 3 presents the calculated lithium ion transference number (t_+) of 0.79 for the phase-inverted TFPE. The initial and steady-state interfacial resistances, both before and after the chronoamperometry test, were obtained via AC-impedance spectroscopy (Tables 3, 4).Incorporating up to 8 *wt*% of mMgO nanofiller into the polymer matrix appears to enhance ion pair dissociation and

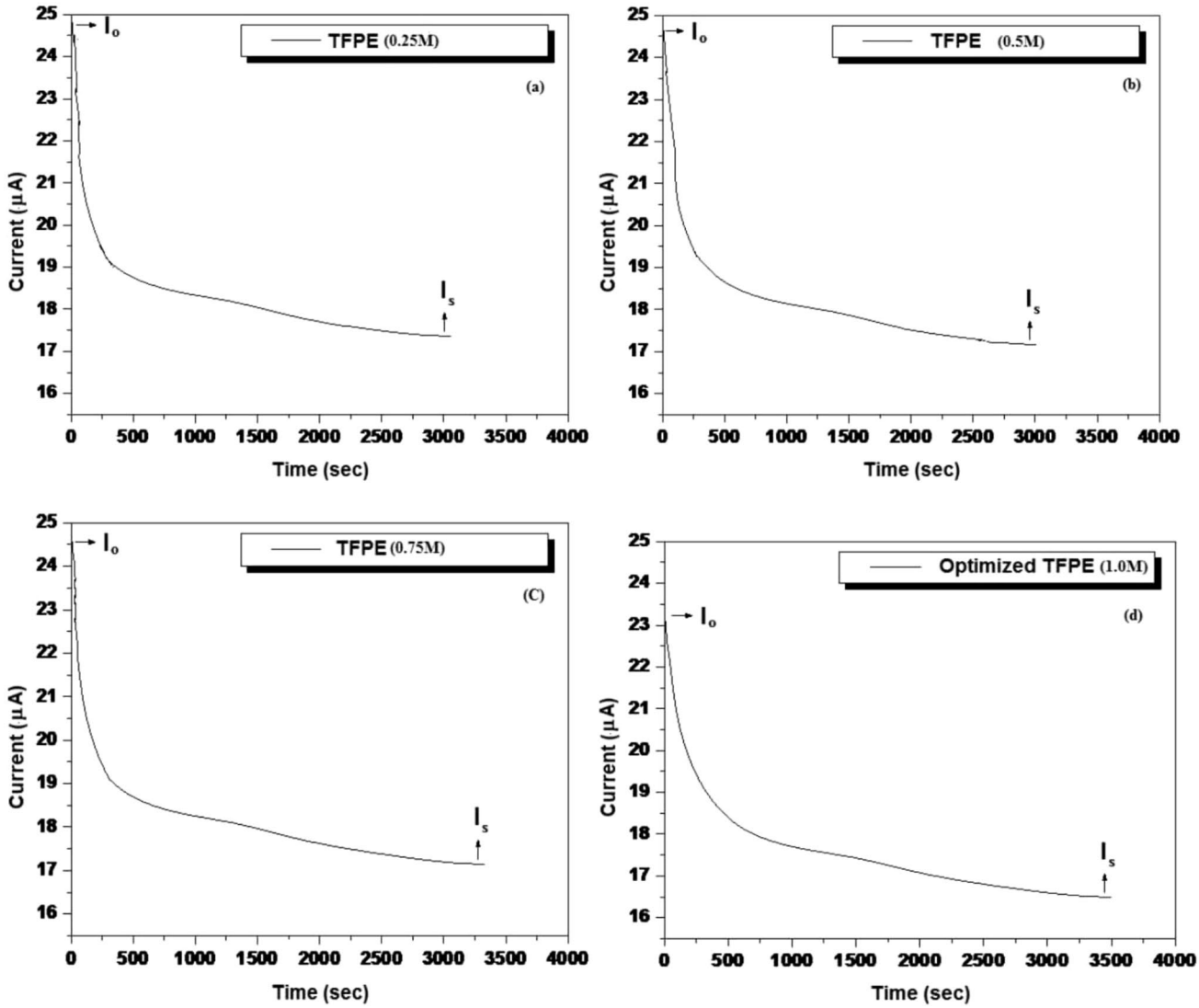


Fig. 16 DC polarization curve of optimized *m*MgO nanofiller in TFPE at different concentration of *y*$LiClO_4$ (y = 0.25 M, 0.5 M, 0.75 M and 1 M)

Table 4 Electrochemical properties of TFPE at various lithum salt concentration

TFPE	σ (mS.cm^{-1})	I_o (μA)	I_s (μA)	R_o (Ω)	R_S (Ω)	Time (sec)	T_+	Film Strength
TFPE1	2.2	24.9	17.7	228.90	397.86	3900	0.58	Excellent
TFPE2	2.3	24.7	17.4	199.12	253.4	3900	0.59	Excellent
TFPE3	2.6	24.6	17.1	168.7	260.3	3700	0.62	Excellent
TFPE4	3.1	23.1	16.5	159.9	226.1	3200	0.79	Excellent

TFPE [92%(PVdF-HFP + 8% *m*MgO + *y*$LiClO_4$ + EC /DMC ((*v*/*v*) 1:1)]; *y*$LiClO_4$ concentration various such as TFPE1, *y* = 0.25 M; TFPE 2, *y* = 0.5 M; TFPE 3, *y* = 0.75 M; TFPE4, *y* = 1 M, respectively

charge carrier mobility, thus improving interfacial stability with lithium electrodes. However, exceeding this concentration leads to reduced transference numbers, likely due to excessive filler accumulation that disrupts the polymer matrix continuity. Moreover, Lithium salt concentration on transference number studies carried out and 1 M $LiClO_4$ was optimized one, and their values were given in Table 4. Transference number (t_+) values lies from minimum (t_+) of 0.58 (TFPE1) to reaches maximum (t_+) of 0.79 (TFPE4) for 0.25 M $LiClO_4$ to 1 M $LiClO_4$ respectively Table 5 has cleared identified that TFPE has better transference number than previous reported values [46].

3.11 Charge and discharge studies

It is crucial to evaluate the cycling performance characteristics of TFPE in the assembled coin-type cells. Electrochemical charge–discharge tests were

Table 5 Comparison of electrochemical study of LiBs with different reported composite polymer electrolytes

Lithium battery electrode/ electrolyte materials	Ionic conductivity σ (S cm^{-1})	Transference number (Li t_+)	Discharge capacity (mAh g^{-1})	References
$LiFePO_4$‖CIME‖Li	1.54×10^{-3} (room temperature)	0.67	145 mAh g^{-1}, (0.2 C), 30 °C	[45]
$LiFePO_4$‖DN-Ionogel‖Lithium 1-ethyl-3methyimidazolium bis(trifluoromethyl)imide–PVDF-HFP ionogel	1.8×10^{-3} (room temperature)	0.33	147.5 mAh g^{-1}, (0.5 C), 30 °C	[46]
$LiFePO_4$‖modified SiO_2 GPE‖Li	1.09×10^{-3} (room temperature)	-	144 mAh g^{-1}, (0.2 C), 25 °C, 100 cycle,	[47]
$LiFePO_4$‖SiO_2-Al_2O_3GPE‖Li	3.2×10^{-3} (room temperature)	-	159.3 mAh g^{-1}, (0.2C), 55 °C, 100 cycle	[48]
LFP‖L-GPE‖Li	8.13×10^{-4} at 40 °C	0.58	148.9 mAh g^{-1}, (0.5C), 90.3% retained, 1000 cycle,	[49]
$LiCoO_2$‖nanoCMPE‖MCMB	2.73×10^{-3}	-	137, 50 cycle, (0.5C)/25 °C	[44]
Al_2O_3-C@NCA‖PVDF-HFP/PPC/Al-LLZO/LiTFSI/SN (Sandwich-PPA) ‖ Li	4.04×10^{-4} (room temperature)	0.583	126.23 mAh g^{-1}, 100 cycle, 80.03% retained, (0.5C) /55 °C	[50]
$LiCoO_2$‖*m*MgO-TFPE‖MCMB	3.1×10^{-3} (room temperature)	0.79	141.9, 50 cycle, 94.6% retained (0.5C) /25 °C	This work

performed using a 2016 coin cell configuration consisting of MCMB||TFPE|| $LiCoO_2$, with TFPE serving as the electrolyte. $LiCoO_2$ was selected due to its widespread application in conventional lithium-ion batteries. The cells underwent galvanostatic cycling with a voltage window set between 3.0 V (lower limit) and 4.2 V (upper limit) at a 0.5C rate. A schematic illustration of the lithium-ion cell setup is depicted in Fig. 17.

The discharge capacities recorded for TFPEs with $LiClO_4$ concentrations of 0.25 M, 0.5 M, 0.75 M, and 1.0 M were 130.6 mAh/g, 131.7 mAh/g, 139.1 mAh/g, and 141.9 mAh/g, respectively. All cycling experiments were performed at a temperature of 25 °C with a constant current density of 0.25 mA cm^{-2} at a C/2 rate. Notably, the cell using 1 M $LiClO_4$ achieved a maximum columbic efficiency of 94.6% by 50th cycle (Fig. 18), outperforming the efficiencies of cells using 0.25 M (91.9%), 0.5 M (92.0%) and 0.75 M (92.7%) $LiClO_4$ of TFPE respectively. It is indicated that the optimum lithium salt concentration significantly impacts discharge capacity. Comparative study of electrochemical performance of LiBs with different reported composite polymer electrolytes performance have given in the Table 5. The $LiCoO_2$ was chosen for its affordability, light weight nature, and attractive

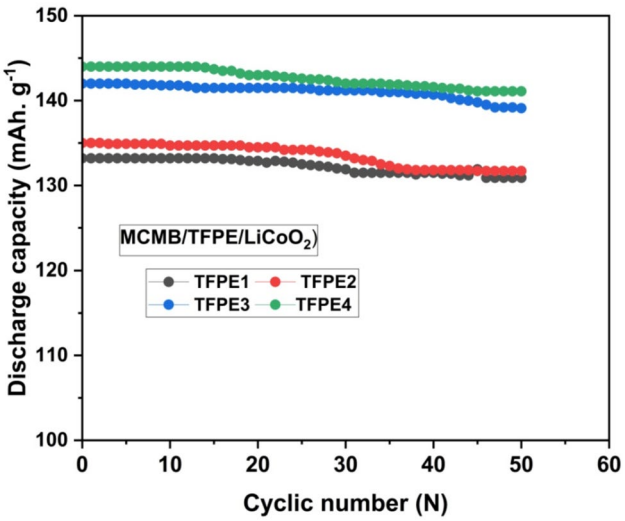


Fig. 18 Relative value of discharge capacity as a function of cycle number of MCMB||TFPE|| $LiCoO_2$ coin type cell

electrochemical properties, including high intercalation voltage and energy density [14]. An optimized TFPE exhibited superior cycling stability, retaining a discharge capacity of 141.9 mAh/g with only 5.4% capacity loss by the 50th cycle, outperforming the other fabricated samples. It clearly indicated that the prepared TFPE4 can be able to use as one of the suitable candidates in lithium- ion batteries.

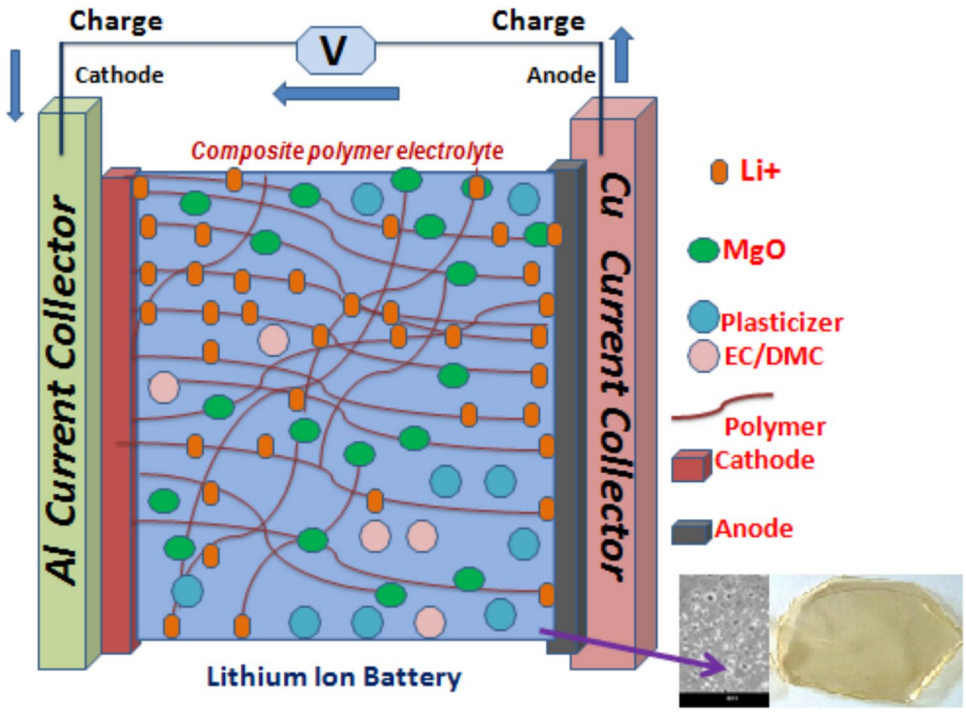


Fig. 17 Schematic representation of LIBs

4 Conclusion

TFPM have been successfully prepared by applying *m*MgO NPs on poly (vinylidenefluoride-co-hexafluoropropylene) (PVdF-HFP) polymer matrix. DSC investigation showed better results in T_m, T_g, ΔH_m and X_c values such as 141.7 °C, − 43.3 °C, 23.84 $J.g^{-1}$ and 22.76% in the optimized TFPM. Incorporation of *m*MgO NPs into the polymer matrix significantly enhances the mechanical strength, reaching up to 2380 kPa. Thin-film polymer membrane electrolytes (TFPEs) were derived from these membranes by immersing into *y*$LiClO_4$ + EC/DMC (1:1 by volume) lithium salt electrolyte solution. The optimized TFPM achieved (81%) maximum porosity, alongside a maximum lithium salt electrolyte uptake of 215%. Ion conductivity of TFPE was obtained 3.1×10^{-3} S cm^{-1} and the Li^+ transference number was found to be a maximum of ca. 0.79. The optimized TFPE employed in MCMB||TFPE||$LiCoO_2$ delivered a discharge capacity of 141.9 mAh/g and also achieved a maximum columbic efficiency of 94.6% by 50th cycle at C/2 rate. These results suggest that the developed TFPEs are promising candidates in future for application in advanced energy storage systems.

Acknowledgements

The authors wish to thanks for the Former Assistant Professor A. Subramana, department of Industrial chemistry, Alagappa University, Karaikudi, India and University Grants Commission (UGC), New Delhi, for giving the constant support to carry out this work. The Authors also expressed sincere thanks to Dr. H J Kim, School of Electrical Engineering, Pusan National University, Jangjeon, Geumjeong, Busan, Republic of Korea and Dr. V. Brinda Sree (TIPS Global Institute) for giving their constant support on the research article work.

Author contributions

G Vijayakumar: Conceptualization, Methodology, Supervision, Data curation, Writing—original draft. B. Rajani: Data curation, Writing—review & editing, N. Sukumar: Conceptualization, Data curation, N Rajiv Chandar—Data curation, Writing—review & editing, V. Sapna: Data curation, P. Selvakumar: Conceptualization, Writing—review & editing and V Tamilavan: Resources, Conceptualization, Methodology, Data curation. M Ponnusamy: Conceptualization.

Funding

This research received no funding.

Data availability

Data will be made available on request.

Declarations

Conflict of interest The authors declare no competing interests.

References

1. H. Liu, F.C. Strobridge, O.J. Borkiewicz, K.M. Wiaderek, K.W. Chapman, P.J. Chupas, C.P. Grey, Batteries. capturing metastable structures during high-rate cycling of $LiFePO_4$ nanoparticle electrodes. Science **34**, 1–7 (2014). https://doi.org/10.1126/science.1252817
2. P. Braun, C. Uhlmann, M. Weiss, A. Weber, I.E. Tiffée, Assessment of all-solid-state lithium-ion batteries. J. Power. Sources **393**, 119–127 (2018). https://doi.org/10.1016/j.jpowsour2018.04.111
3. Y. Wang, J. Yi, Y. Xia, Recent progress in aqueous lithium-ion batteries. Adv. Energy Mater. **2**, 830–840 (2012). https://doi.org/10.1002/aenm.201200065
4. M. Armand, J.M. Tarascon, Building better batteries. Nature **451**, 652–657 (2008). https://doi.org/10.1038/451652a
5. Grand View Research Inc. (2017) Lithium Iron Phosphate ($LiFePO_4$) Material and Battery Market Analysis by Raw Material (Graphite, Lithium Iron Phosphate, Lithium Fluoride), By Application, By Region, And Segment Forecasts, 2014–2025
6. I.T. Kolesnikov, D. Voll, F. Jeschull, P. Theato, Synthesis of polyimide-PEO copolymers: toward thermally stable solid polymer electrolytes for lithium-metal batteries. Eur. Polym. J. **217**, 113315 (2024). https://doi.org/10.1016/j.eurpolymj.2024.113315
7. A. Szczęsna-Chrzan, M. Marczewski, J. Syzdek, M.K. Kochaniec, M. Smoliński, M. Marcinek, Lithium polymer

electrolytes for novel batteries application: the review perspective. Appl Phys A **129**(1), 37 (2023)
8. S.S. Zhang, M.H. Ervin, K. Xu, T.R. Jow, Li-ion battery with poly (acrylonitrile-methyl methacrylate)-based microporous gel electrolyte. Solid State Ionics **176**, 41–46 (2005). https://doi.org/10.1016/j.ssi.2004.05.024
9. N. Farah, H.M. Ng, A. Numan, C.–W. Liew, N.A.A. Latip, K. Ramesh, S. Ramesh, Solid polymer electrolytes based on poly(vinyl alcohol) incorporated with sodium salt and ionic liquid for electrical double layer capacitor. Mater. Sci. Eng. B **251**, 114468 (2019). https://doi.org/10.1016/j.mseb.2019.114468
10. R. Kumar, A. Subramania, N.T. Kalyana Sundaram, G. Vijaya Kumar, I. Baskaran, Effect of MgO nanoparticles on ionic conductivity and electrochemical properties of nanocomposite polymer electrolyte. J. Membr. Sci. **300**, 104–110 (2007). https://doi.org/10.1016/j.memsci.2007.05.014
11. P. Zhang, H.P. Zhang, G.C. Li, Z.H. Li, Y.P. Wu, A novel process to prepare porous membranes comprising SnO2 nanoparticles and P (MMA-AN) as polymer electrolyte. Electrochem. Commun. **10**, 1052–1055 (2008). https://doi.org/10.1016/j.elecom.2008.04.037
12. Z. Su, Z. Yuan, W. He, L. Zhang, Z. Cheng, PVDF-based salt-concentrated polymer electrolyte with high intrinsic lithium salt dissociation capability and ionic conductivity. Ind. Eng. Chem. Res. **64**, 21329–21337 (2025). https://doi.org/10.1021/acs.iecr.5c02722
13. H.-S. Jeong, E.-S. Choi, J.H. Kim, S.–Y. Lee, Potential application of microporous structured poly (vinylidene fluoride-hexafluoropropylene)/poly (ethylene terephthalate) composite nonwoven separators to high-voltage and high-power lithium-ion batteries. Electrochim. Acta **56**, 5201–5204 (2011). https://doi.org/10.1016/j.electacta.2011.03.040
14. A. Subramania, N.T. Kalyana Sundaram, G. Vijayakumar, Structural and electrochemical properties of micro-porous polymer blend electrolytes based on PVdF-co-HFP-PAN for Li-ion battery applications. J. Power. Sources **153**, 177–182 (2006). https://doi.org/10.1016/j.jpowsour.2004.12.009
15. D. Saikia, H.–Y. Wu, Y.C. Pan, C.–P. Lin, K.–P. Huang, K.–N. Chen, G.T.K. Fey, H.–M. Kao, New highly conductive organic–inorganic hybrid electrolytes based on star-branched silica based architectures. Polymer **53**, 6008–6020 (2012). https://doi.org/10.1016/j.polymer.2012.11.012
16. J. Zhang, B. Sun, X. Huang, S. Chen, G. Wang, Honeycomb-like porous gel polymer electrolyte membrane for lithium ion batteries with enhanced safety. Sci. Rep. **4**, 1–7 (2014). https://doi.org/10.1038/srep06007
17. C.M. Costa, L.C. Rodrigues, V. Sencadas, M.M. Silva, J.G. Rocha, S.L. Mendez, Effect of degree of porosity on the properties of poly (vinylidene fluoride–trifluorethylene) for Li-ion battery separators. J. Membr. Sci. **407–408**, 193–201 (2012). https://doi.org/10.1016/j.memsci.2012.03.044
18. V.C. Nguyen, T. Dam, H.-B. Na, C.-J. Park, Plasticized composite electrolyte with Al_2O_3 nanofiller-reinforced PVDF-HFP for solid-state lithium-metal batteries. ACS Appl. Energy Mater. **8**(5), 3120–3313 (2025). https://doi.org/10.1021/acsaem.4c03301
19. H.B. Na, T. Dam, C.J. Park, Sulfonated PVDF-HFP and SiO_2 based quasi-solid-state composite electrolyte for lithium-oxygen batteries. J. Colloid Interface Sci. **15**, 138831 (2026). https://doi.org/10.1016/j.jcis.2025.138831
20. M. Das, K. Ghosh, M.W. Vijaya, Raja, The critical role of Al_2O_3, $BaTiO_3$ and ZrO_2 nanoceramic fillers in PVDF-HFP based composite polymer electrolytes for high performance lithium-metal batteries. Solid State Ionics **430**, 117008 (2025). https://doi.org/10.1016/j.ssi.2025.117008
21. K.H. Khan, A. Zafar, H. Rashid, I. Ahmad, G.S. Khan, H. Hussain, Enhancing lithium-ion conductivity: impact of hausmannite nanofiller on PVDF–HFP/PEG blend nanocomposite polymer electrolytes. Mater. Adv. **5**, 9613–9625 (2024). https://doi.org/10.1039/D4MA00694A
22. D.Y. Song, X. Chen, F.C. Yuan, R.H. Jia, Z. Yan, J.L. Ping, L. Wei, F. Fei, Enhanced thermal and electrochemical properties of PVDF-HFP/PMMA polymer electrolyte by TiO_2 nanoparticles. Solid State Ion. **282**, 31–36 (2015). https://doi.org/10.1016/j.ssi.2015.09.017
23. K.M. Kim, J.M. Ko, N.G. Park, K.S. Ryu, S.H. Chang, Characterization of poly (vinylidene fluoride – co - hexafluoropropylene) - based polymer electrolyte filled with rutile TiO_2 nanoparticles. Solid State Ion. **161**, 121–131 (2003)
24. V.C. Nguyen, T. Dam, H.-B. Na, C.-J. Par, Plasticized composite electrolyte with Al_2O_3 nanofiller-reinforced PVDF-HFP for solid-state Lithium–Metal batteries. ACS Appl. Energy Mater. **8**(5), 3120–3131 (2025). https://doi.org/10.1021/acsaem.4c03301
25. K. Liu, F. Ding, J. Liu, Q. Zhang, X. Liu, J. Zhang, Q. Xu, A cross-linking succinonitrile-based composite polymer electrolyte with uniformly dispersed vinyl-functionalized SiO_2 particles for Li-ion batteries. ACS Appl. Mater. Interfaces **8**, 23668–23675 (2016). https://doi.org/10.1021/acsami.6b05882
26. D. Lin, W. Liu, Y. Liu, H.R. Lee, P.C. Hsu, K. Liu, Y. Cui, High ionic conductivity of composite solid polymer electrolyte via in situ synthesis of monodispersed SiO_2

nanospheres in poly (ethylene oxide). Nano Lett. **16**, 459–465 (2016). https://doi.org/10.1021/acs.nanolett.5b04117

27. G. Vijayakumar, S.N. Karthick, R. Paramasivam, C. Ilamaran, Morphology and electrochemical properties of P (VdF-HFP)/MgO-based composite microporous polymer electrolytes for Li-ion polymer batteries. Polym.-Plast. Technol. Eng. **51**, 1427–1431 (2012). https://doi.org/10.1080/03602559.2012.706864
28. G. Vijayakumar, S.N. Karthick, A. Subramania, New class of P (VdF-HFP)–CeO_2–$LiClO_4$-based composite microporous membrane electrolytes for Li-Ion batteries. Int. J. Electrochem. **926383**, 1–10 (2011). https://doi.org/10.4061/2011/926383
29. N. Zebardastan, M.H. Khanmirzaei, S. Ramesh, K. Ramesh, Novel poly (vinylidene fluoride-co-hexafluoro propylene)/polyethylene oxide based gel polymer electrolyte containing fumed silica (SiO_2) nanofiller for high performance dye-sensitized solar cell. Electrochim. Acta **220**, 573–580 (2016). https://doi.org/10.1016/j.electacta.2016.10.135
30. K. Karuppasamy, H.W. Rhee, P.A. Reddy, D. Gupta, L. Mitu, A.R. Polu, S.X. Shajan, Ionic liquid incorporated nanocomposite polymer electrolytes for rechargeable Lithium ion battery: a way to achieve improved electrochemical and interfacial properties. J. Ind. Eng. Chem. **40**, 1–9 (2016). https://doi.org/10.1016/j.jiec.2016.06.020
31. K. Karuppasamy, P.A. Reddy, G. Srinivas, A. Tewari, R. Sharma, X.S. Shajan, D.J. Gupta, Electrochemical and cycling performances of novel nonafluorobutanesulfonate (nonaflate) ionic liquid based ternary gel polymer electrolyte membranes for rechargeable Lithium ion batteries. J. Membr. Sci. **514**, 350–357 (2016). https://doi.org/10.1016/j.memsci.2016.05.010
32. M. Forsyth, D.R. Macfarlane, A. Best, J. Adebahr, P. Jacobsson, A.J. Hill, The effect of nano-particle TiO_2 fillers on structure and transport in polymer electrolytes. Solid State Ion. **147**, 203–211 (2002). https://doi.org/10.1016/S0167-2738(02)00017-6
33. Y. Li, J. Wang, J. Tang, Y. Liu, Y. He, Conductive performances of solid polymer electrolyte films based on PVB/$LiClO_4$ plasticized by PEG200, PEG400 and PEG600. J. Power. Sources **187**, 305–311 (2009). https://doi.org/10.1016/j.jpowsour.2008.11.126
34. H.J. Woo, S.R. Majid, A.K. Arof, Effect of ethylene carbonate on proton conducting polymer electrolyte based on poly (ε-caprolactone) (PCL). Solid State Ionics **252**, 102–108 (2013). https://doi.org/10.1016/j.ssi.2013.07.005
35. S. Schantz, L.M. Torell, J.R. Stevens, Ion pairing effects in poly (propylene glycol)–salt complexes as a function of molecular weight and temperature: a Raman scattering study using NaCF3SO3 and LiClO4. J. Chem. Phys. **94**, 6862–6867 (1991). https://doi.org/10.1063/1.460265
36. M. Deepa, S. Agnihotry, D. Gupta, R. Chandra, Ion-pairing effects and ion–solvent–polymer interactions in LiN (CF3SO2) 2–PC–PMMA electrolytes: a FTIR study. Electrochim. Acta **49**, 373–383 (2004). https://doi.org/10.1016/j.electacta.2003.08.020
37. H. Teherpuria, S. Mohapatra, A.K. Meel, S.S.P. Chowdhury, S. Kanchi, P.K. Jaiswal, S. Mogurampelly, Ionic conductivity mechanisms in PEO–$NaPF_6$ electrolytes. Nanoscale **17**, 21573–21581 (2025). https://doi.org/10.1039/D5NR01630D
38. P. Kumari, S.A. Hashmi, Highly flexible and electrochemically stable Mg-ion conducting gel polymer electrolyte based on PVdF-HFP/PMMA blend for application in magnesium batteries. J. Energy Storage **111**, 115389 (2025). https://doi.org/10.1016/j.est.2025.115389
39. K A Filsinger, A Dasgupta and C B Arnold, (2020) Fluorinated Alkoxyaluminates As Electrolytes for Calcium-Ion Batteries, The Electrochemical Society, *Meet. Abstr.* https://doi.org/10.1149/MA2020-022223mtgabs.
40. Z. Wang, H. Yang, S. Cai, D. Zhang, Z. Guo, Enhancing the performance of alkaline aluminum-air batteries with polyoxyethylene diamine and calcium citrate as compound additives. J. Energy Storage **134**, 118094 (2025). https://doi.org/10.1016/j.est.2025.118094
41. F. Chen, X. Wang, M. Armand, M. Forsyth, Cationic polymer-in-salt electrolytes for fast metal ion conduction and solid-state battery applications. Nat. Mater. **21**(10), 1175–1182 (2022). https://doi.org/10.1038/s41563-022-01319-w
42. A. Subramania, G.V. Kumar, A.R.S. Priya, T. Vasudevan, Polyol-mediated thermolysis process for the synthesis of MgO nanoparticles and nanowires. Nanotechnology **18**(22), 225601–225605 (2007). https://doi.org/10.1088/0957-4484/18/22/225601
43. S. Wang, J. Hu, X. Gui, S. Lin, Y. Tu, A promising PMMA/m-MgO all-solid-state electrolyte for lithium-oxygen batteries. J. Electrochem. Soc. **168**, 020514 (2021). https://doi.org/10.1149/1945-7111/abdfa6
44. G. Vijayakumar, N.R. Chandar, V. Tamilavan, Z. Said, R. Paramasivam, Physical and charge discharge behavior of facile PVDF-HFP nanocomposite microporous polymer electrolyte for lithium ion polymer batteries. J. Mater. Sci. Mater. Electron. **33**, 8594–8606 (2022). https://doi.org/10.1007/s10854-021-06622-x
45. Y.F. Tang, Y. Xiong, L. Wu, X. Xiong, T. Me, X. Wan, A solid-state lithium battery with PVDF–HFP-modified fireproof ionogel polymer electrolyte. ACS Appl. Energy Mater. **6**(7), 4016–4402 (2023). https://doi.org/10.1021/acsaem.3c00249

46. L. Liang, X. Chen, W. Yuan, H. Chen, H. Liao, Y. Zhang, Highly conductive, flexible, and nonflammable double-network poly(ionic liquid)-based ionogel electrolyte for flexible lithium-ion batteries. ACS Appl. Mater. Interfaces **13**(21), 25410–25420 (2021). https://doi.org/10.1021/acsami.1c06077
47. X. Li, M. Zhang, J. He, D. Wu, J. Meng, P. Ni, Effects of fluorinated SiO_2 nanoparticles on the thermal and electrochemical properties of PP nonwoven/PVdF-HFP composite separator for Li-ion batteries. J. Membr. Sci. **455**, 368–374 (2014)
48. M. Li, Y. Liao, Q. Liu, J. Xu, P. Sun, H. Shi, W. Li, Application of the imidazolium ionic liquid based nano-particle decorated gel polymer electrolyte for high safety lithium ion battery. Electrochim. Acta **284**, 188–201 (2018). https://doi.org/10.1016/j.electacta.2018.07.140
49. T. Zhao, Q. Gai, X. Deng, J. Ma, H. Gao, A new type of LATP doped PVDF-HFP based electrolyte membrane with flame retardancy and long cycle stability for solid state batteries. J. Energy Storage **73**, 108576 (2023). https://doi.org/10.1016/j.est.2023.108576
50. H.K. Tran, B.T. Truong, B.-R. Zhang, R. Jose, J.-K. Chang, C.-C. Yan, Sandwich-structured composite polymer electrolyte based on PVDF-HFP/PPC/Al-doped LLZO for high-voltage solid-state lithium batteries. ACS Appl. Energy Mater. **6**(3), 1475–2148 (2023). https://doi.org/10.1021/acsaem.2c03363

Publisher's Note Springer Nature remains neutral with regard to jurisdictional claims in published maps and institutional affiliations.

Springer Nature or its licensor (e.g. a society or other partner) holds exclusive rights to this article under a publishing agreement with the author(s) or other rightsholder(s); author self-archiving of the accepted manuscript version of this article is solely governed by the terms of such publishing agreement and applicable law.